DOI: 10.13009/EUCASS2023-588
Aerospace Europe Conference 2023 – 10TH EUCASS – 9TH CEAS

Analysis of the structural behaviour of wings with nonlinear components for passive load reduction

Daniel Hahn[1,2,†], *Lennart Lobitz*[1,2], *Matthias Haupt*[1,2] *and Sebastian Heimbs*[1,2]
[1] *Cluster of Excellence SE*^{2}*A - Sustainable and Energy-Efficient Aviation, Technische Universität Braunschweig*
[2] *Institute of Aircraft Design and Lightweight Structures (IFL), Technische Universität Braunschweig*
Hermann-Blenk-Str. 35, D-38108 Braunschweig, Germany
daniel.hahn@tu-braunschweig.de
[†]Corresponding author

Abstract

Structural analyses of modified wing structures are performed to achieve nonlinear progressive tip twisting behaviour for passive load reduction by exploiting buckling of selected components. In this paper, wing box segments with a previously developed design concept are integrated into a full three-dimensional finite element model of the wing. Parametric analyses are performed to find a good design and corresponding sensitivities. The result is a wing design for future aeroelastic analysis that utilizes the modified wing box segments to induce additional wing twisting, potentially improving the load reduction behaviour above a critical load compared to a conventional design.

1. Introduction

The structural weight of the wing contributes significantly to the weight of an aircraft. Lighter aircraft allow for fuel savings and emissions reductions. Reducing the weight of one component has a snowball effect, allowing weight savings in other components. For example, a reduction in gross weight by reducing the weight of the wings allows for smaller engines. This in turn reduces gross weight and lift requirements, allowing for smaller and lighter wings. Wing weight reduction thus contributes to energy-efficient and environmentally friendly aviation. Wing weight depends on the amount of material needed to withstand aerodynamic and internal loads. Lift is the essential load for the aircraft to fly. It is equal to the weight of the airplane in level flight. Lift is distributed over the wing and contributes to the internal bending moment at the wing root. During manoeuvres such as turns or vertical speed changes, the lift differs from the aircraft weight by the load factor n_z. In typical turns with a bank angle of 30°, the load factor is $n_z = 1.15$. Changes in vertical speed, such as takeoff, are performed with a similar load factor for passenger comfort. The airplane is required to maintain a larger $n_z = 2.5$ if it is aerodynamically possible to generate that lift. At low airspeeds, such high lift may not be aerodynamically possible because of the high angle of attack required in slow flight. To increase lift, the angle of attack must be increased. At a critical angle of attack, the flow separates and no lift is produced, which is called a stall. At high speeds, such as cruise, lower angles of attack are required to produce the necessary lift. Therefore, the wing does not stall until $n_z = 2.5$ and it is aerodynamically possible to generate this lift.

Load control or load alleviation aims to reduce the maximum loads occurring on the wing. The reduction is achieved by shifting the lift distribution towards the wing root, reducing the bending moment, or reducing the total possible load factor. Load reduction techniques are divided into active and passive techniques. The current generation of passenger aircraft uses active load alleviation by deflecting the ailerons to reduce lift in the outboard wing during high load cases [1]. New developments for active load alleviation are directed towards improved actuation by fluidic [2] or piezoelectric actuators [3]. The implementation of forward-looking LIDAR sensors is being investigated to improve the actuation control behaviour [4].

The basic idea of passive load reduction is to design the structure so that high loads deform the structure in a lift-reducing manner due to fluid-structure interaction. One way to achieve lift reduction is to introduce bending-twist coupling, which reduces the angle of attack in the outboard wing as it bends, thus shifting the lift toward the wing root. A method to achieve this is aeroelastic tailoring [5]. Aeroelastic tailoring uses specific directional stiffness distributions such as specially designed composite lay-ups [6] or skewed stiffeners [7]. It is used not only for load reduction but also for cruise efficiency [8] and flutter suppression [9]. Alternative concepts to achieve load reduction are hinged wingtips [10]. A semi-passive method uses the temperature-dependent stiffness of components that are electrically

DOI: 10.13009/EUCASS2023-588

heated to the desired stiffness [11]. For dynamic gust loads, damping elements at the strut-wing joint of strut-braced wings also reduce loads by damping the motion [12].

Several concepts studied for passive load reduction exploit structural nonlinearities to generate load-reducing deformations that progressively increase with load. Such concepts are the implementation of multistable composite elements with snap-through behaviour to abruptly change the stiffness distribution at a critical load [13, 14], negative stiffness spring devices for hinged wingtips [15], and box beam spars with buckling rear web to increase bending-twist coupling [16].

The present study originates from a project in the Cluster of Excellence SE^{2}A" *Sustainable and Energy-Efficient Aviation*", which aims to explore such innovative nonlinear concepts with high fidelity fluid-structure interaction methods for transonic transport aircraft. The nonlinearity chosen for this project is buckling. This is similar to bistable elements, but is less abrupt and does not require actuation of the element to return to its original state. When the component buckles at a critical load in the range of $n_z = 1.2$ to $n_z = 1.5$, the stiffness distribution of the wing changes and the acting fluid forces deform the wing. To reduce lift, this deformation must reduce the effective angle of attack. This can be achieved by downward twisting and airfoil changes. A wing box segment with a nonlinear progressive bending torsion coupling has been designed by the authors [17]. This segment twists the outboard wing downwards under high load. The mechanisms are tailored skin layups in the unstiffened upper skin, which buckle like a tilted hinge, combined with rear spar buckling.

This study involves the integration of these previously developed wing box segment modifications into a full wing model and the analysis of its structural behaviour. The loads are based on a 1g load case and scaled to higher loads. Nonlinear aerodynamics and aerodynamic response to deformation are not considered at this time. However, the purpose of this study is to size the nonlinear structures and explore the behaviour under general high loading conditions in order to develop a design that can be used as a starting point in coupled fluid-structure interaction simulations.

Section 2 covers the analysis methods. In section 3 the concept of wing modification is presented. Sections 4 and 5 show the results of quasi-stationary loads such as manoeuvring loads for one and two modified rib bays. Dynamic loads representing discrete gusts according to the certification specification are presented in section 6. Conclusions are presented in section 7.

2. Methods

The analyses in this study are performed using the commercial finite element toolbox *Abaqus*. This section first describes the process used to create the baseline wing model and then describes the analysis procedures used to perform quasi-stationary and dynamic analyses of the behaviour of the modified wing.

2.1 Initial wing sizing

The wing model for the modifications analysed in this paper was generated with an in-house parametric tool using the *Common Parametric Aircraft Configuration Schema (CPACS)* [18] and associated geometry library *TiGL* [19]. The parametric wing geometry including structural components can be exported in STEP format using *TiGL* and then imported into *Abaqus* where a finite element model is automatically built.This process includes assigning properties, discretising and applying loads and boundary conditions. Shell elements are used to model surfaces, while beam elements are used to model stiffeners such as stringers, spar caps, rib caps and vertical stiffeners. Load cases are derived from conceptual aircraft design studies of the SE^{2}A reference aircraft by Karpuk et al. [20]. The loads are applied as concentrated forces at the rib nodes. The magnitude takes into account a spanwise load distribution and a normalised chordwise 2D pressure distribution, which are interpolated to obtain the local force.

The tool also includes methods for dimensioning the wing structures according to an iterative fully stressed design approach, similar to the approach used in Sommerwerk et al. [21]. In this approach, a failure index is calculated for each sizing criterion, shell, and stiffener. The failure index is equal to 0 when the component is unloaded and equal to 1 when the loading is equivalent to the allowed maximum loading. At the end of each iteration, the wall thickness of each shell and stiffener is adjusted based on their critical failure index. The primary structure of the wing investigated in this study consists of quasi-isotropic laminates of carbon fibre reinforced polymers (CFRP). The Puck failure criterion is used to evaluate fibre and inter-fibre failure [22]. Linear stability analyses are performed to derive failure indices for buckling in each panel. The initial design must prevent local buckling of skin panels up to the limit load and global buckling up to the ultimate load. Von Mises stresses are used to evaluate the strength failure of the beam stiffener.

Tables 1 and 2 give the elastic and strength-related material properties used for the unidirectional layers in the laminates of the primary wing structure and the isotropic properties used to model the beam stiffeners.

DOI: 10.13009/EUCASS2023-588

Table 1: Elastic properties of IM6EP in a unidirectional (UD) ply and a quasi-isotropic (QI) layup.

Type	$\mathbf{E_1}$ **/ GPa**	$\mathbf{E_2}$ **/ GPa**	$\mathbf{G_{12}}$ **/ GPa**	ν_{12}	ρ / $\frac{\mathrm{kg}}{\mathrm{m}^3}$
UD	177.0	10.8	7.6	0.27	1600
QI	75.3	75.3	26.9	0.40	1600

Table 2: Strength properties of IM6EP in a unidirectional (UD) ply and a quasi-isotropic (QI) layup.

Type	X_t **/ MPa**	X_c **/ MPa**	Y_t **/ MPa**	Y_c **/ MPa**	**S / MPa**	$\mathbf{R}_{p0.2}$ **/ MPa**
UD	2860	1875	49	246	83	-
QI	-	-	-	-	-	624

2.2 Quasi-stationary analysis

In order to evaluate and adapt the behaviour of the modified wing to conditions with loads above the 1g cruise load, quasi-stationary analyses are performed. Since the goal of this study is to exploit the nonlinear behaviour in the load regime above 1g, geometric nonlinearities are considered in these analyses. In a steady-state analysis, a stationary equilibrium between external and restoring forces is required. Buckling, as used in the concept of this paper, can lead to numerical difficulties in establishing a stationary equilibrium near bifurcation loads. To avoid these difficulties, this study uses a quasi-stationary analysis, which is a dynamic analysis where the load is applied so slowly that inertia effects are not relevant to the overall behaviour. It is only during the buckling events that inertia allows convergence to a dynamic equilibrium. Decaying oscillations occur immediately after a buckling event and are part of the dynamic simulation. They are damped by numerical dissipation and Rayleigh material damping. The Rayleigh damping coefficients are set to $\alpha = 1$ (mass proportional) and $\beta = 0.001$ (stiffness proportional).
As shown in Hahn and Haupt [17], aerodynamic pressure loads on the skin can significantly affect the buckling shape. For this reason the loads are applied as surface forces on the skin surfaces instead of concentrated forces on the ribs as used for the initial wing sizing in section 2.1. The pressure distribution is obtained by the same interpolation between the spanwise load distribution in the 1g cruise case at Ma = 0.71 and 7650 m altitude from the SE^2A reference aircraft [20] and a chordwise pressure distribution on the DLR-F15 airfoil calculated with 2D-CFD. For higher loads, such as manoeuvring loads, this pressure distribution is scaled proportionally to the desired factor. A change in the qualitative pressure distribution due to aerodynamic or aeroelastic effects is not considered in this analysis.
The load is scaled up to 2 g, which is less than the typical 2.5 g. The reasons are that the SE^2A reference aircraft designs [20] assume a maximum load factor of 2 g, which is enabled by various assumed load alleviation mechanisms. Since the response of the aerodynamic pressure loads to the deformation is not considered in this paper, 2.5 g would overestimate the loads on the wing. For the quasi-stationary analysis the 2 g load is applied in the dynamic analysis within 100 s.
The primary result data is the wing tip twist θ at the trailing edge at each time step. This data is supplemented by the wing tip trailing edge translation u_z for each time step and the field data of the displacements of all nodes for selected time points. The gradient of rotation due to load and buckling loads for specific buckling events are derived from the primary data.

2.3 Dynamic gust encounter

Inertia effects can change the behaviour in fast loading conditions. This is relevant for gust load cases because gust encounters are short, especially at cruise speed. For this reason, the behaviour of the wing structure is also evaluated under simulated gust loading conditions. The gust lengths and vertical velocities are based on the certification requirements. The vertical velocity profile in time and space is a 1-cos gust. Since fluid simulation is not performed in this study, the corresponding transient behaviour of the load factor history is estimated by considering the change in angle of attack $\Delta\alpha$ and the slope of the lift curve $C_{L\alpha} = \mathrm{d}C_L/\mathrm{d}\alpha$. The ratio between the actual lift coefficient C_L and the lift coefficient at cruise speed $C_{L,cruise}$ is the load factor. The equation is

$$n_z(t) = 1 + \frac{\Delta\alpha(t) \cdot C_{L\alpha}}{C_{L,cruise}} \tag{1}$$

In a stationary situation $\Delta\alpha$ can be calculated by $\arctan(w_g/V)$ with the vertical gust velocity w_g and the true airspeed V. If used in a transient model, this would assume instantaneous lift development. However, the fluid is also influenced by inertial effects that result in a certain lift build-up time or effective angle of attack. To account for these effects, a

DOI: 10.13009/EUCASS2023-588

convolution approach using Küssner's function is used as described in Wright and Cooper [23]. Küssner's function $\Psi(\tau)$ describes the lift response to a step $\Delta\alpha$ and is calculated with

$$\Psi(\tau) = \frac{\tau^2 + \tau}{\tau^2 + 2.82\tau + 0.8} \tag{2}$$

where τ is the normalised time calculated by $\tau = 2tV/c$ and $\tau = 1$ is the time taken to travel half the chord distance. The chord is represented by c and the physical time by t. The effective vertical velocity $w_{g,kuessner}$ for a vertical velocity profile other than a step can be determined by the convolution integral of the derivative of the Küssner function (corresponding to the impulse response) $\Psi' = \mathrm{d}\Psi/\mathrm{d}\tau$ and the vertical velocity profile w_g.

$$w_{g,kuessner}(\tau) = \int_0^\tau w_g(\tau_0) \cdot \Psi'(\tau - \tau_0)\mathrm{d}\tau_0 \tag{3}$$

The effective angle of attack for load factor estimation is calculated from the convoluted vertical velocity using

$$\Delta\alpha(t) = \arctan\left(\frac{w_{g,kuessner}(\tau(t))}{V}\right). \tag{4}$$

The vertical velocity profiles according to the certification specification CS25.341 range from gust lengths between 18 m and 214 m and maximum vertical velocities between 10.77 m/s (18 m gust) and 16.26 m/s (214 m gust). The parameters are based on the mission profile of the reference aircraft mission profile [20] and are summarised in table 3.

Table 3: Mission parameters for dynamic analyses.

Parameter	**Value**	**Unit**
V	220	m/s
c	4.1	m
$C_{L,cruise}$	0.31	-
$C_{L\alpha}$	0.0962	deg^{-1}

These parameters used in the procedure described result in the load factor histories shown in figure 1. The gust encounter analysis simulates 10 s, starting from a steady state solution at 1g load. This initial steady state is obtained using the static solver available in *Abaqus*. The provided automatic stabilisation is used to overcome possible small local instabilities. As in the quasi-stationary analyses, the primary result data is the wing tip displacement, supplemented by wing tip translation and field data of the entire model at selected time points.

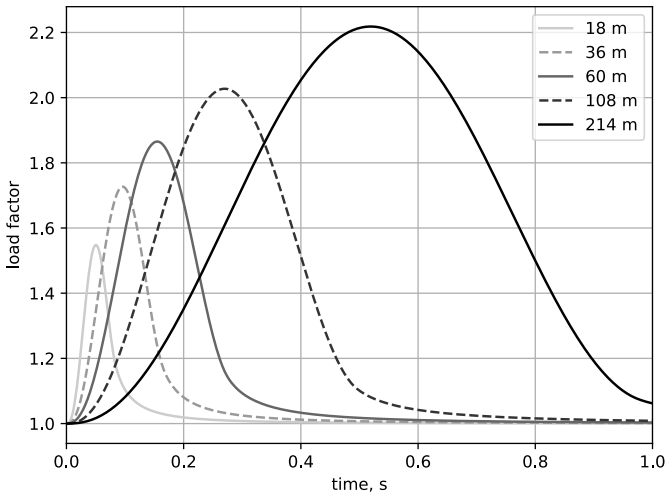

Figure 1: Load factor histories for dynamic gust simulations.

DOI: 10.13009/EUCASS2023-588

3. Wing structure modification

The wing structure is modified to allow for progressive tip twisting at loading conditions above 1.2 g. The authors developed a basic concept for the wing modification on a simplified wing box segment model in previous work [17]. The resulting concept is briefly summarised and implemented in the full wing model in this section.

3.1 Nonlinear components

The concept developed by the authors of the present paper in previous work [17] is based on buckling shell components and tailoring of anisotropic stiffness. Buckling is chosen because of the significant nonlinearity in stiffness. To allow for buckling, stiffeners such as stringers are removed. The shell thickness is then increased to match the buckling to the desired load level.
Two components are selected for buckling. The first component is the upper skin. Upper skin buckling introduces additional bending due to reduced upper skin stiffness in the post-buckling regime. This bending is similar to a hinge activated at the buckling load. For backward swept wings like the one considered here, the increased bending already introduces downward tip twist due to the geometry. To further increase the downward twist, the directional stiffness of the skin is designed so that the longitudinal axis of the bulge is tilted relative to the flow direction during buckling. Thus, the hinge-like behaviour acts like a tilted hinge, providing additional tip twist in the deformed state. Load reduction techniques based on real hinges have been studied by Castrichini et al. [15]. The directional anisotropic stiffness is introduced by the use of tailored fibre composite layups. Previous work by the authors [17] found a layup of $[35/\text{-}55/45/\text{-}45]_s$ with ply thickness fractions of (45 %, 15 %, 20 %, 20 %), where 0° coincides with the wing box axis, to provide the desired buckling behaviour.
The second component is the rear spar. When it buckles, the stiffness is reduced and the shear centre of the wing box moves forward. This allows for additional tip twisting under load. The composite ply layup found advantageous in previous work [17] is a $[40/\text{-}40]_{2S}$ balanced ply layup with equal thickness fractions for the plies.

3.2 Application in the wing model

The basic concept described in section 3.1 is incorporated into the complete wing model created by the procedure described in section 2.1. The modification is not applied to the entire wing box. It is only applied to up to two segments at about 65 % of the wing span. This position is chosen because the load reduction is particularly effective in the outer wing due to the large contribution to the bending moment due to the large lever arm. Further inside the wing, the required skin thicknesses may become very large due to the high loads in the inner wing, which may limit the buckling capabilities. In addition, a larger part of the wing would have to be moved, which could affect the reaction time. On the other hand, a position further out would limit the effective area for load reduction. For these reasons the position at 65 % of the span is chosen. This position is not changed in the present study. Further investigation could be aimed at optimising the position of the modification.

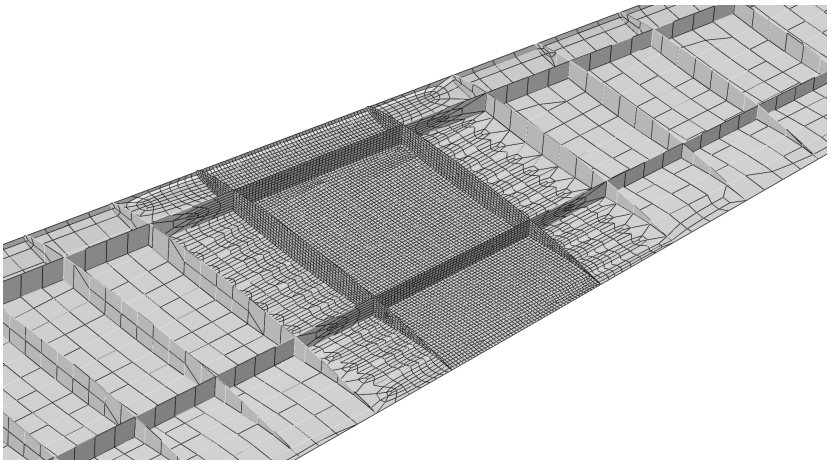

Figure 2: Modified mesh for the wing with one modified rib bay (upper skin hidden).

As in section 3.1, all stiffeners in the edited section are removed. To have compliant adjacent leading and trailing edges, their stiffeners are also removed. To allow for larger skin panels with improved targeted buckling behaviour, two rib

DOI: 10.13009/EUCASS2023-588

bays are combined into one modified rib bay by removing the centre rib. This changes the aspect ratio of the modified rib bays compared to the unmodified rib bays. The basic layup is based on the section 3.1. Thickness sizing and related behaviour analysis is the subject of this paper and is covered in detail in sections 4 and 5. It covers both the single rib bay and double rib bay designs.
The finite element grid in the modified rib bay is significantly refined to allow good representation of the buckling bulges. The adjacent rib bays are used to transition from the coarse wing model to the refined edited rib bay. The mesh is shown in figure 2. This increases the number of elements. The unmodified base model has 13,013 elements. The model with one modified rib bay has 27,086 elements and the model with two modified rib bays has 38,057 elements. The skin, spar and ribs are linear shell elements. The stiffeners, such as stringers and caps, outside the edited area are linear beam elements. Since the objective of this study is to investigate the wing deformations enabled by buckling and to develop a design to analyse this load alleviation concept in terms of aeroelastic behaviour considering fluid-structure interaction in future work, the material model is simplified. In particular, material failure criteria are not considered at this stage.

4. Quasi-stationary analyses with one modified rib bay

This section presents the parametric analyses to find the best design with only one modified rib bay and evaluates the sensitivities to different design variables. The design variables are the shell thicknesses of the skins and spars.

4.1 Influence of skin thickness

The first parameter variation concerns the thickness of the upper skin in the modified rib bay segment. In these calculations the ratios between spars and skin thicknesses are kept constant and are taken from the results of previous work [17]. The rear spar thickness is 31 % of the upper skin and the front spar thickness is 47 % of the upper skin. By increasing the upper skin thickness, the spars are sized accordingly. The upper skin thickness range considered in this analysis is 8 mm - 13 mm.
The load factor-twist curves of all calculated thicknesses are shown in figure 3. For small loads below the first occurrence of skin buckling, all variants show the same linear relationship. The different buckling loads for the different skin thicknesses can be identified by the horizontal step in twist at a given load. The step is followed by decaying oscillations, which are due to the dynamic simulation technique and are not of interest in this quasi-stationary consideration. At higher loads, the twist continues with a smaller slope. This can be seen as a decreasing torsional stiffness after the buckling event. However, since the load case composed of a pressure distribution with shear, bending and torsional components is more complex than a single torsional load, it is not exactly the torsional stiffness of the structure. This behaviour is desired for the proposed load reduction concept because it results in increased downward twisting and thus a reduction in the angle of attack after the buckling load.

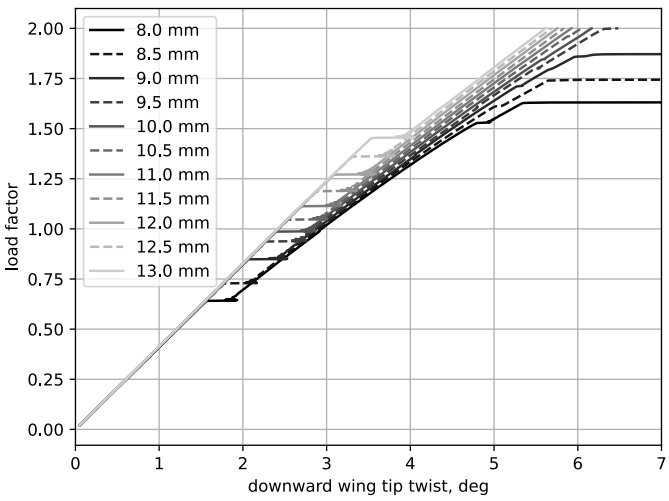

Figure 3: Downward wing tip twist for different upper skin thicknesses (spars and lower skin scaled accordingly).

DOI: 10.13009/EUCASS2023-588

The case with a skin thickness of 12 mm has a buckling load of 1.27 g, which best meets the requirements of the load reduction starting between 1.2 g and 1.5 g as defined in section 1. The wing deformation at different load factors is shown in figure 4 together with a detail of the buckled upper skin. It can be seen that in addition to the increased twisting after buckling, there is also increased wing bending.

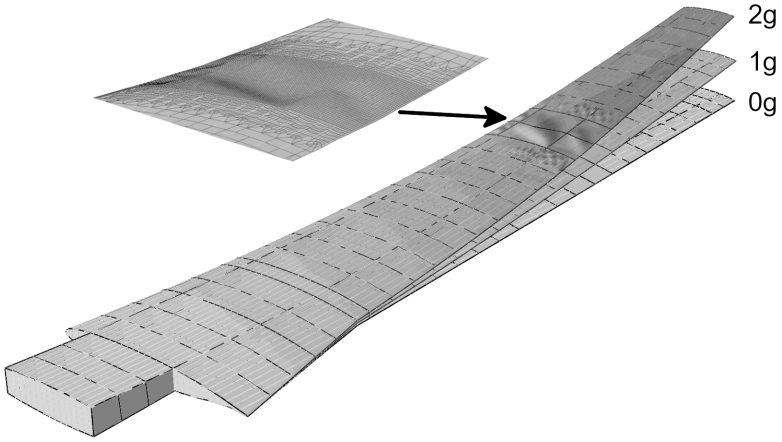

Figure 4: Deformed wing at 0 g, 1 g and 2 g in the post-buckling regime with 12 mm skin thickness.

Variants with lower thicknesses achieve greater wing twisting at 2 g, but their buckling load is below the defined minimum buckling load of 1.2 g for manoeuvring. The variants with thicknesses below 10 mm have not only one but several significant nonlinearities. At load factors above 1.5 g, the spars collapse in an unstable wrinkle mode, causing the wing to snap upwards. The load is not supported by this mode of the post-buckled structure, so the simulation procedure stops and the structure would fail regardless of the material properties. Such behaviour is shown in figure 5. These variants cannot be used for the load reduction concept because a stable post-buckling regime is required.

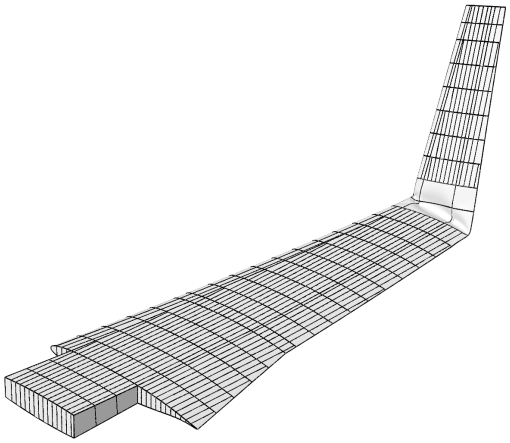

Figure 5: Undesirable spar collapse due to insufficient shell thickness shown for 8 mm skin thickness.

If higher buckling loads than 1.27 g are desired, a skin thickness greater than 12 mm can be selected. This is at the expense of less downward twist. In any case, a post-buckled structure will achieve more downward twist than a linear extrapolation of the twist gradient of the pre-buckled behaviour.

4.2 Influence of rear spar thickness

In previous work [17] the rear spar supported the twist when it buckled in a shear mode. In order to find the best rear spar thickness for the application in the present wing, model variations with rear spar thicknesses between 17.5 % and 45 % of the skin thickness are investigated. Since the model with a skin thickness of 12 mm from section 4.1 is the most promising candidate, it is used as the basis for this variation. Therefore, the thickness of the rear spar is varied between 2.1 mm and 5.4 mm.

DOI: 10.13009/EUCASS2023-588

The results are shown in figure 6. Except for the variants with thickness less than 25 % of the skin thickness, the rear spar thickness has very little influence on the buckling load and post-buckling behaviour. The buckling load of all variants between 17.5 % and 45 % differs by 0.012 g. The tip twist of the variation between 25 % and 45 % differs by 0.1° between 5.72° and 5.82°. Below 20 % thickness ratio, the spar buckles in wrinkling mode, leading to the unstable collapse also seen in section 4.1 and figure 5.

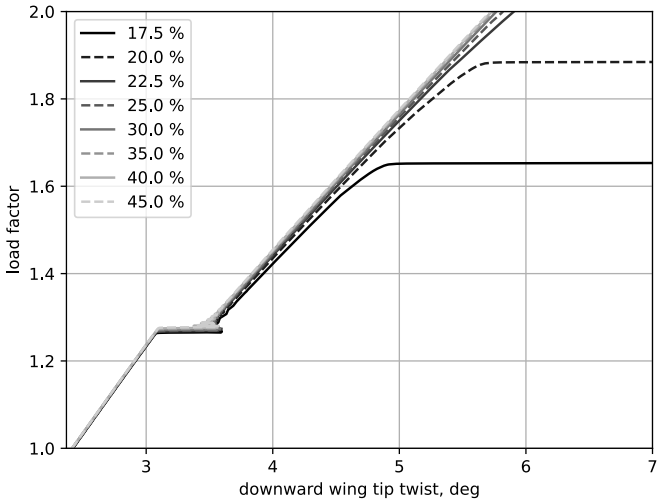

Figure 6: Downward wing tip twist for different rear spar thickness ratios to 12 mm upper skin thickness.

Contrary to the results of previous work [17], the rear spar modification does not significantly contribute to the wing twisting, but can be used to control and prevent the wrinkling mode. Since in this study the wrinkling mode only occurs in the cases below 22.5 %, the selected design is 30 %. There are some differences between the wing box model in the previous work [17] and the wing analysed in this paper. The wing box model is based on an earlier version of the SE^{2}A medium range reference configuration, which affects the aspect ratios and load assumptions. In particular, the height of the wing box is greater in the earlier version, which makes the aspect ratio of the spars thinner in the newer version. In addition, the full wing model has a trailing edge attached to the rear spar. These differences may be the reason for the current reduced significance of rear spar buckling in the full wing model.

5. Quasi-stationary analyses with two modified rib bays

To further increase the tip twisting, a second modified rib bay is added to the wing and is located next to the first modification on the inboard side. This section of the paper shows the corresponding analyses of the mutual influences of the two modified and buckling segments, discusses the sensitivities, and provides a design with the desired nonlinear twisting behaviour at loads higher than 1.2 g.

5.1 Influence of the second modified rib bay

Similar to section 4.1, the upper skin thickness of the second modified rib bay (hereafter called the inner rib bay) is varied between 14 mm and 22 mm. The values in this range are larger than for the first modification (hereafter called the outer rib bay) because of its position closer to the fuselage, which experiences larger bending moments. The outer wing box is constructed like the best design from section 4 with a skin thickness of 12 mm and a rear spar thickness of 30 % of the skin thickness.
Figure 7 shows the results of this parameter study. In general, the behaviour is similar to the analysis of the outer rib bay in figure 3. The different buckling loads of the inner rib bay and the increased wing twist at 2 g are visible. Only the model with the smallest skin thickness of 14 mm shows buckling of the outer rib bay at a load factor of 1.88 g. This clearly shows the influence of the inner rib bay buckling on the outer rib bay buckling load. Without inner rib bay buckling, the outer rib bay buckles at 1.27 g according to section 4. The buckling of the inner rib bay changes the boundary conditions and internal loads for the outer rib bay. For the inner rib bay, an upper skin thickness of 16 mm is selected for the design as the buckling load is 1.23 g and meets the criteria.

DOI: 10.13009/EUCASS2023-588

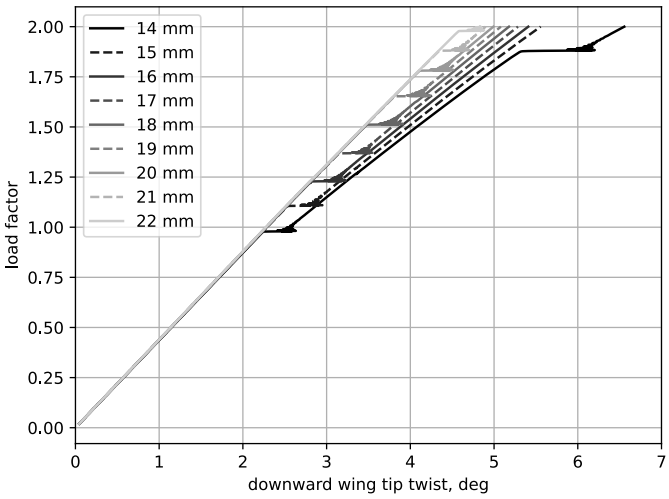

Figure 7: Downward wing tip twist for different upper skin thicknesses of the inner modified rib bay segment (upper skin thickness of the outer modified rib bay segment: 12 mm, rear spar ratio: 30 %).

5.2 Resizing of the first modified rib bay

As noted in section 5.1, the selected skin thickness of the outer rib bay of 12 mm will no longer cause the outer rib bay to buckle below 2 g if the inner rib bay is also sized to buckle. Therefore, the skin thickness of the outer rib bay is reduced. The series starts with a minimum thickness of 8 mm and scales up to 11.5 mm.

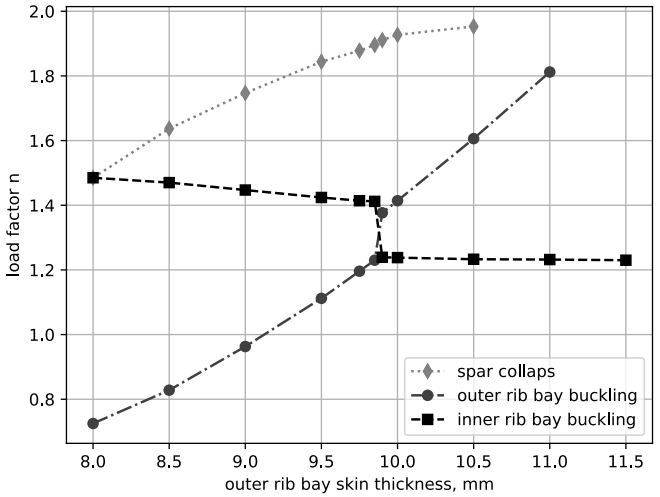

Figure 8: Buckling loads of outer and inner modified rib bay segments, and spar collapse loads for different outer rib bay upper skin thicknesses (spars scaled accordingly).

The resulting buckling loads for the corresponding rib bays are shown in figure 8. Additionally, the collapse mode load is included in the figure. The results show that in this configuration it is not possible to find a skin thickness where the buckling loads of both rib bays are equal. The buckling load factor of increasing outer rib bay thickness increases approximately linearly in the range studied. Between 9.85 mm and 9.9 mm, this linear increase is interrupted by a jump of 0.15 g as the first buckling rib bay changes from the outer rib bay to the inner rib bay. The inner rib bay with a skin thickness of 16 mm buckles at load factors between 1.5 g and 1.4 g as the outer rib bay buckles at lower loads. It decreases from 1.5 g to 1.4 g as the buckling load of the outer skin increases. At the critical skin thickness where the

DOI: 10.13009/EUCASS2023-588

first rib bay buckles, the buckling load for the inner rib bay jumps to 1.23 g. This is the load it was originally designed for in section 5.1, where the outer rib bay buckles at higher loads. Since the design is supposed to buckle between 1.2 g and 1.5 g, the 9.9 mm case just after the switch load is selected for the design. The reason for having the outer rib bay buckle first is that it affects less of the wing. Small loads require less load reduction than large loads. Therefore, the inner rib bay contributes to the load reduction at higher critical loads.
With two buckling rib bays, the selected spar size of the rear spar is no longer sufficient to prevent the wing from entering the collapse mode at loads below 2 g in almost all cases up to 10.5 mm. This occurs in the thinner outer rib bay.

5.3 Spar modification

Section 5.2 has shown that without further changes to the structure, it enters the wrinkling mode below 2 g, which is not feasible. As shown in section 4.2, strengthening the rear spar can improve this behaviour without significantly affecting the desired tip twist. Therefore, in this last quasi-stationary analysis of this paper, the thickness of the outer wing box is again modified. The skins are sized to 9.9 mm in the outer rib bay and 14 mm in the inner rib bay. The rear spar of the inner rib bay is sized to be 30 % of the corresponding skin thickness, which is 4.2 mm. The rear spar of the outer rib bay varies between 25 % and 40 % of the corresponding skin thickness in this series of models. In absolute units, this is approximately 2.5 mm - 4 mm.

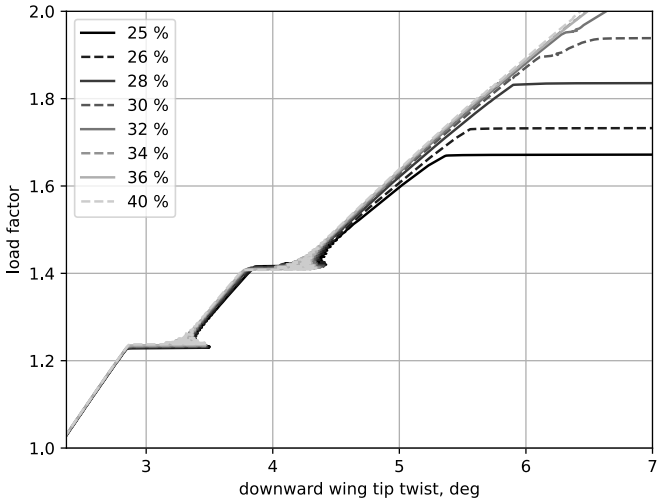

Figure 9: Downward wing tip twist for different rear spar thickness ratios of the outer rib bay to a skin thickness of 9.85 mm.

Figure 9 shows the resulting tip twisting behaviour. The results are consistent with the expectations of the behaviour in section 4.2, so no further differences due to the second buckling rib bay can be identified by this parametric study. The first model to prevent instability or buckling mode collapse is the one with 34 % spar to skin ratio. Since the differences in buckling loads and twisting at 2 g are negligible between 34 % and 40 %, 40 % is chosen for the design to provide some safety margin against collapse mode.

5.4 Resulting design

This section presents the design developed for further investigation. The inner modified rib bay has an upper skin thickness of 14 mm and a rear spar thickness ratio of 30 %. The outer modified rib bay has an upper skin thickness of 9.9 mm and a rear spar thickness ratio of 40 %. Figure 10 shows the final model at 0 g, 1 g and 2 g with nonlinear calculation both enabled and disabled for reference. Both modified rib bays are in the post-buckling state at 2 g and the difference between the post-buckling deformation and the linear reference is clearly visible. The top left hand corner of the figure contains the tip twist behaviour with respect to the 1 g case. The buckling loads are 1.24 g for the outer and 1.41 g for the inner rib bay. The difference in twist gradient and absolute twist values compared to the linear reference is significant. The maximum twist increase compared to the 1 g twist for the nonlinear version is 4.14°. The twist in the

DOI: 10.13009/EUCASS2023-588

linear reference is only 2.29°. So the twist is increased by a factor of 1.8 or a difference of 1.85° due to the nonlinear components. Using $\Delta n_z = \Delta\alpha \cdot C_{L\alpha}/C_{L,cruise}$ the local load factor reduction at the wing tip with $\Delta\alpha = 1.85°$ is 0.59. This is only a rough estimate, since the twist difference decreases towards the wing, and the interaction of deformation and load is not covered in this investigation.

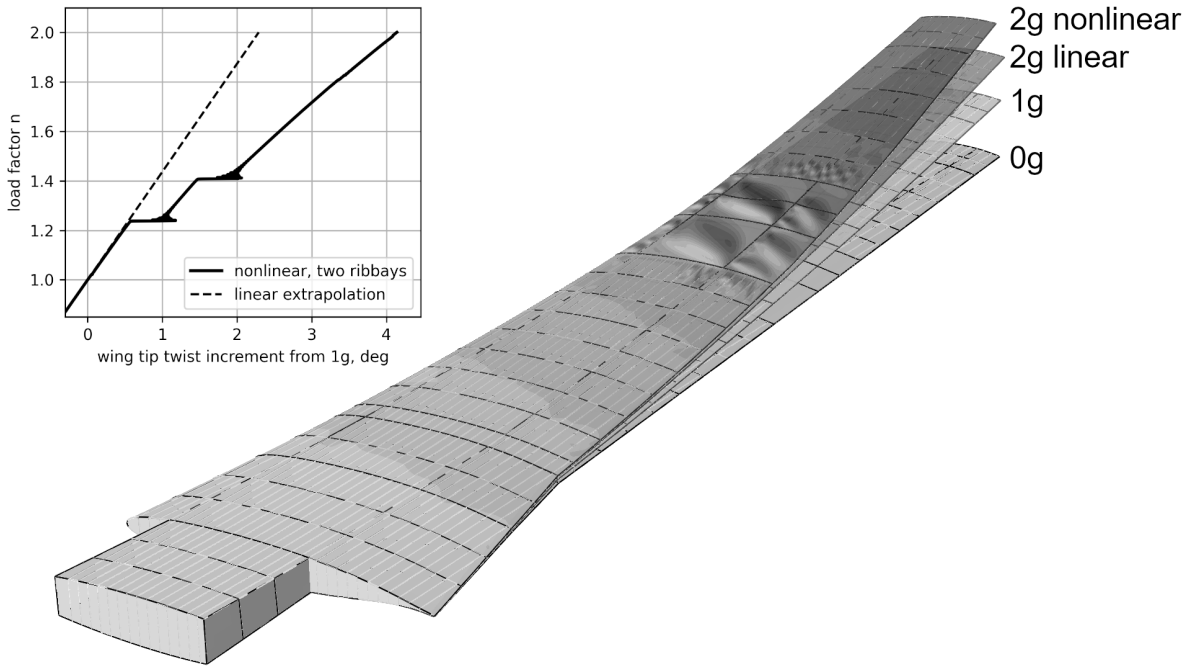

Figure 10: Deformation and wing twisting behaviour of the final parameter selection with a linear reference.

6. Dynamic analyses

Previous work by the authors [24] on 2D airfoils with camber change due to buckling stiffeners showed some limitations due to delayed response due to inertia. For this reason, dynamic gust simulations according to the procedure described in 2.3 are performed with the selected design. However, as this is not a coupled simulation and therefore neglects not only the quasi-stationary load reduction but also drag and aerodynamic damping, the general behaviour in terms of amplitudes may differ significantly from a coupled analysis.

The resulting tip twisting with respect to time is shown in figure 11. The plot shows data from the first second of the simulation, which contains the first and largest peaks of all gusts and all structural responses. Oscillations are excited in all gusts. The twist peak of the two short gusts is well after the peak vertical velocity with 0.095 s and 0.089 at gust durations of 0.08 s and 0.16 s, respectively. At peak vertical velocity, the twist change is only 0.43° in the 18 m gust and 1.01° in the 36 m gust. By the time the twist peak is reached, the load factor has decreased to 1.04 g in the 18 m gust and 1.11 g in the 36 m gust. The influence of inertia is therefore significant in these short gusts and limits any possible load reduction, since the gust passes almost completely before the twist peak. Beginning with the 60 m gust, the gust frequency moves into the range of the structure's natural frequency of about 3 Hz. In addition, the time difference between the structure and the gust peak becomes smaller as the gust length increases. This means that the peaks become quite close to each other with respect to the gust arrival time. The structural peak in the 60 m gust has the largest value because it is closest to the resonance frequency. There is still some delay in this gust with a difference of 0.071 s. In the 108 m gust the difference drops to 0.015 s. The twist at the peak of the gust is 5.97° and the load at the peak of the twist is 2.02 g. The 214 m gust is similar. The twist peak is actually reached before the gust peak because of the superimposed oscillation. The twist at the gust peak is 5.19° and the load at the twist peak is 2.2 g. Due to the approximate nature of this analysis without aeroelastic response, these values are not the values that will occur in a coupled system where there is additional aerodynamic damping. These calculations still show that less effective load reduction can be expected in the fast gusts due to inertia. In the longer gusts, which also have higher peak loads, inertia has less influence and more effective load reduction can be expected.

DOI: 10.13009/EUCASS2023-588

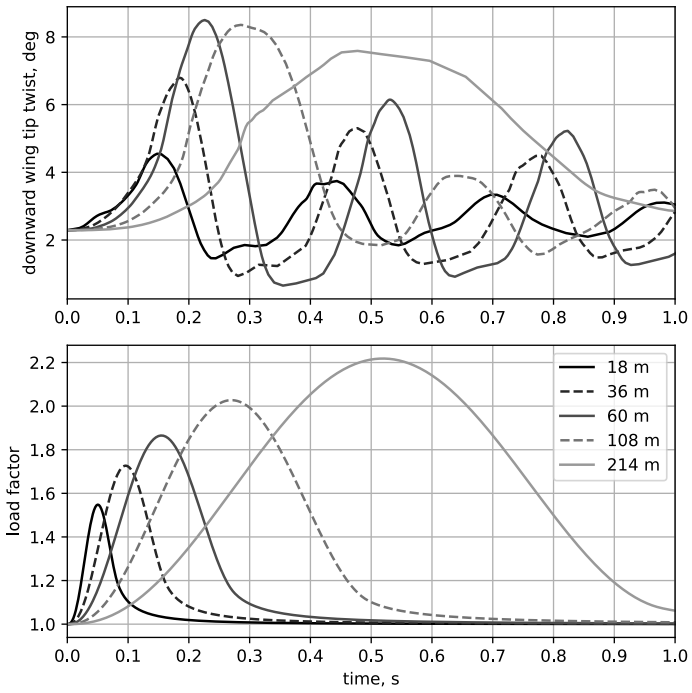

Figure 11: Downward wing tip twist and load factor in different gust lengths.

7. Conclusions

This paper presents structural analyses of a wing design that incorporates components to achieve progressive nonlinear twisting behaviour. The base component developed in a previous paper by the authors [17] is a rib bay with tailored upper skin composite and no stringers, which is designed to buckle at a given critical load and enter a post-buckling mode with a tilted bulge acting like a hinge. Additional twisting is achieved in the previous study by also exploiting the rear spar buckling.

The present paper extends these previous investigations by including the concept in a full wing model instead of analysing only a simplified rib bay. In general, the concept is shown to provide the desired additional wing twist. The rib bay to be buckled has a larger rib spacing than the rest of the wing to achieve an approximately square aspect ratio and improve the buckling mode. The component sizing needs to be adjusted and is analysed in this paper. It is found that for the given wing, rear spar buckling does not contribute significantly to the observed wing twisting. Instead, increasing the thickness of the rear spar helps to prevent the wing from entering an unstable higher buckling mode where the spars buckle in a wrinkling mode. Wing twisting can be further increased by using a second modified rib bay. The skin thicknesses must be carefully matched because the buckling loads of the rib bays influence each other. The buckling loads of the two rib bays are not equal. One rib bay buckles first and increases the buckling load of the other by changing the boundary and load conditions. In the wing design proposed in this paper, the outer rib bay buckles first. If more modified rib bays are used, the rear spar of the first buckling rib bay may need to be further strengthened, as is the case in the proposed wing design. Dynamic calculations show that inertia is expected to limit the load reduction capabilities in shorter gusts, while no significant inertia limitations are expected in the longer gust.

The analyses in this paper approximate the loading conditions and do not include the changing loads in response to the deformation. The purpose of the analyses is to find a suitable design with the desired behaviour. In future studies, this design will be analysed in simulations that include fluid-structure interaction to evaluate the actual load reduction capabilities.

Acknowledgements

We would like to acknowledge the funding by the Deutsche Forschungsgemeinschaft (DFG, German Research Foundation) under Germany's Excellence Strategy **EXC 2163/1** - Sustainable and Energy Efficient Aviation - **Project ID 390881007**

DOI: 10.13009/EUCASS2023-588

References

[1] C. D. Regan and C. V. Jutte. Survey of applications of active control technology for gust alleviation and new challenges for lighter-weight aircraft. NASA, Dryden Flight Research Center, Edwards, California, 2012, https://ntrs.nasa.gov/archive/nasa/casi.ntrs.nasa.gov/20120013450.pdf, Accessed 03.08.2020.

[2] S. Asaro, K. Khalil, and A. Bauknecht. Unsteady characterization of fluidic flow control devices for gust load alleviation. In Andreas Dillmann, Gerd Heller, Ewald Krämer, and Claus Wagner, editors, *New Results in Numerical and Experimental Fluid Mechanics XIII*, volume 151 of *Notes on Numerical Fluid Mechanics and Multidisciplinary Design*, pages 153–163. Springer International Publishing, Cham, 2021.

[3] A. C. Henry, G. Molinari, J. R. Rivas-Padilla, and A. F. Arrieta. Smart morphing wing: Optimization of distributed piezoelectric actuation. *J. Intell. Mater. Syst. Struct.*, 57(6):2384–2393, 2019.

[4] N. Fezans and H.-D. Joos. Combined feedback and LIDAR-based feedforward active load alleviation. In *AIAA Atmospheric Flight Mechanics Conference*, Grapevine, Texas, 2017. American Institute of Aeronautics and Astronautics.

[5] M. H. Shirk, T. J. Hertz, and T. A. Weisshaar. Aeroelastic tailoring - Theory, practice, and promise. *Journal of Aircraft*, 23(1):6–18, 1986.

[6] W R Krüger, J Dillinger, R. de Breuker, and K. Haydn. Investigations of passive wing technologies for load reduction. *CEAS Aeronautical Journal*, 10(4):977–993, 2019.

[7] A. Abdelkader, M. Harmin, J. Cooper, and F. Bron. Aeroelastic tailoring of metallic wing structures. In *52nd AIAA/ASME/ASCE/AHS/ASC Structures, Structural Dynamics and Materials Conference*, Denver, Colorado, 2011. American Institute of Aeronautics and Astronautics.

[8] G. A. A. Thuwis, R. de Breuker, M. M. Abdalla, and Z. Gürdal. Aeroelastic tailoring using lamination parameters. *Structural and Multidisciplinary Optimization*, 41(4):637–646, 2010.

[9] O. O. Bendiksen. Recent developments in flutter suppression techniques for turbomachinery rotors. *Journal of Propulsion and Power*, 4(2):164–171, 1988.

[10] A. Castrichini, V. Hodigere Siddaramaiah, D. Calderon, J. E. Cooper, T. Wilson, and Y. Lemmens. Nonlinear folding wing-tips for gust loads alleviation. In *56th AIAA/ASCE/AHS/ASC Structures, Structural Dynamics, and Materials Conference*, Kissimmee, Florida, 2015.

[11] W. Raither, M. Heymanns, A. Bergamini, and P. Ermanni. Morphing wing structure with controllable twist based on adaptive bending-twist coupling. *Smart Materials and Structures*, 22(6):065017, 2013.

[12] C. P. Szczyglowski, S. A. Neild, B. Titurus, J. Z. Jiang, J. E. Cooper, and E. Coetzee. Passive gust loads alleviation in a truss-braced wing using integrated dampers. In *International Forum on Aeroelasticity and Structural Dynamics, IFASD*, Como, Italy, 2017.

[13] A. F. Arrieta, I. K. Kuder, M. Rist, T. Waeber, and P. Ermanni. Passive load alleviation aerofoil concept with variable stiffness multi-stable composites. *Composite Structures*, 116:235 – 242, 2014.

[14] W. D. K. Cavens, A. Chopra, and A. F. Arrieta. Passive load alleviation on wind turbine blades from aeroelastically driven selectively compliant morphing. *Wind Energy*, 24(1):24–38, 2021.

[15] A. Castrichini, J. E. Cooper, T. Wilson, A. Carrella, and Y. Lemmens. Nonlinear negative stiffness wing-tip spring device for gust loads alleviation. In *AIAA 15th Dynamics Specialists Conference*, San Diego, California, 2016.

[16] F. Runkel, U. Fasel, G. Molinari, A. F. Arrieta, and P. Ermanni. Wing twisting by elastic instability: A purely passive approach. *Composite Structures*, 206:750 – 761, 2018.

[17] D. Hahn and M. Haupt. Exploration of the effect of wing component post-buckling on bending-twist coupling for nonlinear wing twist. *CEAS Aeronautical Journal*, 13(3):663–676, 2022.

[18] M. Alder, E. Moerland, J. Jepsen, and B. Nagel. Recent advances in establishing a common language for aircraft design with CPACS. In *Aerospace Europe Conference 2020*, Bordeaux, France, 2020.

DOI: 10.13009/EUCASS2023-588

[19] M. Siggel, J. Kleinert, T. Stollenwerk, and R. Maierl. TiGL: An open source computational geometry library for parametric aircraft design. *Mathematics in Computer Science*, 13(3):367–389, 2019.

[20] S. Karpuk, R. Radespiel, and A. Elham. Assessment of future airframe and propulsion technologies on sustainability of next-generation mid-range aircraft. *Aerospace*, 9(5):279, 2022.

[21] K. Sommerwerk, I. Krukow, M. Haupt, and D. Dinkler. Investigation of aeroelastic effects of a circulation controlled wing. *Journal of Aircraft*, 53(6):1746–1756, 2016.

[22] A. Puck and H. Schürmann. Failure analysis of FRP laminates by means of physically based phenomenological models. *Composites science and technology*, 62(12-13):1633–1662, 2002.

[23] J. R. Wright and J. E. Cooper. *Introduction to aircraft aeroelasticity and loads*. AIAA education series. Wiley, Chichester, 2008.

[24] D. Hahn, M. Haupt, and S. Heimbs. Load alleviation capabilities of wings with nonlinear structural behavior in stationary and dynamic load cases. In *International Forum on Aeroelasticity and Structural Dynamics, IFASD*, Madrid, Spain, 2022.